ISSN 1063-7842, Technical Physics, 2019, Vol. 64, No. 1, pp. 86–91. © Pleiades Publishing, Ltd., 2019.
Russian Text © A.A. Dmitrievskii, A.O. Zhigachev, D.G. Zhigacheva, A.I. Tyurin, 2019, published in Zhurnal Tekhnicheskoi Fiziki, 2019, Vol. 89, No. 1, pp. 107–111.

SOLID STATE

Structure and Mechanical Properties of the $CaO–ZrO_2–Al_2O_3$ Ceramic Composites at Low Corundum Concentrations

A. A. Dmitrievskii[a,*], A. O. Zhigachev[a], D. G. Zhigacheva[a], and A. I. Tyurin[a]

[a] *Derzhavin Tambov State University, Tambov, 392000 Russia*

**e-mail: aadmitr@yandex.ru*

Received March 5, 2018

Abstract—We have studied the effect of the ratio between concentrations of zirconium dioxide (stabilized by CaO) and corundum on phase composition and mechanical properties of nanostructured $CaO–ZrO_2–Al_2O_3$ ceramic composites. The $CaO–ZrO_2–Al_2O_3$ composites sintered at temperatures typical of ZrO_2 are found to be characterized by the optimal microhardness/fracture toughness ratio at corundum content $C_{Al_2O_3} = 5\%$. These composites have a high flexural strength; their porosity, coefficient of friction, and wear are typical of those for $CaO–ZrO_2$ ceramics.

DOI: 10.1134/S1063784219010092

INTRODUCTION

The requirements posed to the performance characteristics of structural materials by the consumer market are being constantly tightened. With respect to structural ceramics, the efforts made by research and development engineers mainly focus on improving hardness, fracture toughness, and wear resistance, as well as on reducing porosity and the coefficient of friction. The performance characteristics of ceramics can be improved by varying the ratio between concentrations of the initial components and synthesis variables. Unfortunately, materials with increased hardness tend to have reduced ability to resist crack formation and propagation under mechanical load. One of the most efficient ways to avoid this effect is to design composite materials. An additive incorporated into the matrix aims to significantly improve some parameters, while the other ones are either negligibly deteriorated or not affected at all.

The greatest success has been achieved by combining stabilized zirconium dioxide, which is characterized by record-high flexural and impact strength among all oxide ceramic materials, and corundum, which is characterized by high hardness [1–3]. Although the general relationship between hardness and fracture toughness is retained, this method allows one to produce $ZrO_2–Al_2O_3$ ceramic composites with high mechanical properties (Fig. 1) [2, 4–11]. Hardness of the resulting composite is enhanced by adding fine-grained corundum particles into the matrix of stabilized zirconium dioxide. Fracture toughness may go down not very significantly, since reduction of the content of material ensuring transformation strengthening (ZrO_2) [11–13] within the composite is partially compensated for by dispersion strengthening [13] due to increased Al_2O_3 concentration. However, the higher corundum content in the composite makes it necessary to increase the sintering temperature [14]. This change in process increases the average grain size of ZrO_2, having a negative effect on hardness. In addition, the sintering process becomes more complex and expensive. Therefore, searching for the optimal ratios between ZrO_2 and Al_2O_3 concentrations and synthesis variables (grinding and sintering conditions in particular) has been a rather relevant task for many years. Dmitrievskii et al. [15], demonstrated that two-phase synthesis at relatively low temperatures ($T_1 = 1300$°C, $T_2 = 1200$°C) and at low corundum contents ($C_{Al_2O_3} \sim 5\%$) yields $CaO–ZrO_2–Al_2O_3$ ceramic composite characterized by high hardness and fracture toughness.

The extensive use of zirconium ceramics and composites based on it as a material for fabricating wearing pieces (units of constructions and devices subjected to friction while in operation) makes such tribological properties as the coefficient of friction and wear very important. In this connection, our study was aimed at investigating the structure and a complex of mechanical and tribological properties of the $CaO–ZrO_2–Al_2O_3$ ceramic composite synthesized by low-temperature sintering depending on corundum concentration.

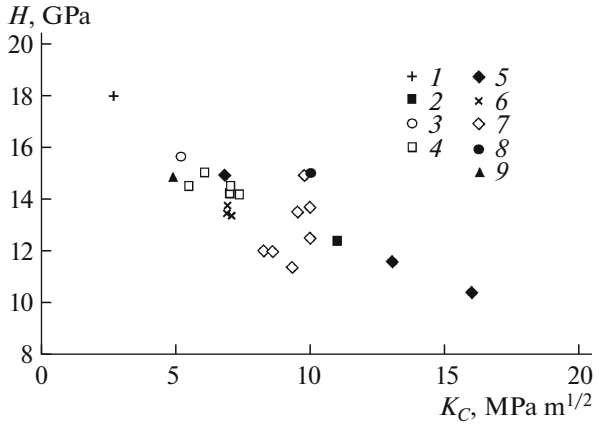

Fig. 1. The ratio between hardness and fracture toughness of ZrO_2–Al_2O_3 ceramic composites differing in terms of concentrations of their components and synthesis conditions: (*1*) [4]; (*2*) [5]; (*3*) [6]; (*4*) [7]; (*5*) [8]; (*6*) [9]; (*7*) [10]; (*8*) [2]; and (*9*) [11].

EXPERIMENTAL

Composite components, the powders of synthetic zirconium dioxide, calcium oxide, and corundum, were mixed in the following way. The molar concentration of the stabilizer (CaO) with respect to ZrO_2 remained unchanged (C_{CaO} = 6.5 mol %), while the mass concentration of Al_2O_3 with respect to the CaO–ZrO_2 mixture was varied within the range 0–25 wt %. The resulting powder mixtures were dispersed in distilled water at a 1 : 1 weight ratio and subjected to ultrasound homogenization. Next, the mixture was ground in a planetary ball mill for 5 h. The components of the composite and grinding bodies were taken at a 1 : 5 ratio. After grinding, the mixture was dried in a furnace at T_0 = 80°C for 24 h. The specimens were molded by uniaxial dry pressing at a load of 5000 kg for 30 s.

The specimens were sintered in air in the two-stage mode. At the first stage, the specimens were heated at a constant rate (5°C/min) to temperature T_1 = 1300°C and kept under these conditions for 5 min. Next, they were cooled down to temperature T_2 = 1200°C and sintered for 4 h. Cooling to room temperature was performed at a rate 5°C/min. According to the findings reported in [15], this sintering mode is optimal in terms of the resulting mechanical properties for the CaO–ZrO_2–Al_2O_3 ceramic composite with low corundum content.

The prepared specimens were studied to reveal the effect of corundum concentration on their structure (phase composition, average grain size D, and porosity Π) and physicomechanical and tribological properties (microhardness H, fracture toughness K_C, flexural strength σ_{max}, Young's modulus E, coefficient of friction μ, and wear W) of the synthesized ceramic composites. The specimens to be used for testing microhardness, fracture toughness, and Young's modulus were molded together with thermoplastic material and subjected to mechanical polishing and buffing.

Porosity Π was determined using standard formula

$$\Pi = (1 - \rho_v/\rho_t) \times 100\%. \quad (1)$$

where ρ_t is the theoretical density of the composite with allowance for corundum content and ρ_v is the density of the composite measured by underwater weighing.

The Vickers hardness H (microhardness) test was performed on an automated Duramin-A300 microhardness tester at a load of 50 N. The Young's modulus, coefficient of friction, and degree of wear were tested using a Triboindenter TI 950 nanoindenter. An Axio Observer A1m metallographic inverted microscope equipped with a Structure 5.0 image analyzer was used to visualize the indenter marks and measure lengths of radial cracks formed at the indenter mark. Fracture toughness K_C was determined using expression (2) according to the procedure described in [16]:

$$K_C = k\left(\frac{E}{H}\right)^{\frac{1}{2}}\frac{P}{l^{\frac{3}{2}}}, \quad (2)$$

where P is the maximum indenter load; l is the length of radial cracks at the indenter mark; and k is an empirical calibration coefficient ($k = 0.016 \pm 0.004$).

A three-point bending flexural test was conducted using an MTS 870 Landmark pull-test machine. Flexural strength σ_{max} was determined from expression (3):

$$\sigma_{max} = \left(\frac{3FL}{2ab^2}\right), \quad (3)$$

where F is the test-failure load; L is the specimen (bar) length; and a and b are the width and thickness of the specimen, respectively.

The ratio between the force of resistance to relative motion of indenter upon friction (lateral force F_L) and the normal component of the response of external forces F_N acting on the body surface at the contact zone was a measure used to estimate coefficient of friction μ upon scribing:

$$\mu = \left(\frac{F_L}{F_N}\right). \quad (4)$$

The data on phase composition and the average grain size were obtained using a D2 Phaser XRD diffractometer. The structure of the ceramic composite (the distribution of corundum crystallites over the CaO–ZrO_2 matrix) and the pattern of propagation of radial cracks at indenter marks were visualized using a high-resolution scanning electron microscope (Carl Zeiss).

RESULTS

Phase Composition, Crystallite Size, and Porosity

According to the data summarized in Table 1, most zirconium (91–98%) in the composite has a tetragonal structure in the entire analyzed range of corundum

Table 1. Structural parameters and the phase composition of a $CaO–ZrO_2–Al_2O_3$ ceramic composite with different corundum concentrations

$C_{Al_2O_3}$, %	Phase composition			Structural parameters		
	C_{m-ZrO_2}	C_{t-ZrO_2}	C_{c-ZrO_2}	D_{ZrO_2}, nm	$D_{Al_2O_3}$, nm	Π, %
0	0	91	9	65	–	2.8
2.5	0	98	2	75	–	2.7
5	2	96	2	85	–	0.6
10	1	95	4	80	75	0.3
12.5	2	92	6	85	120	0.5
25	2	91	7	85	100	0.7

concentrations (CAl_2O_3 = 0–25%). The contents of monoclinic and cubic phases of zirconium dioxide vary within the ranges of 0–2% and 2–9%, respectively. The highest content of the tetragonal phase (C_{t-ZrO_2} = 98%) was detected when corundum concentration in composite $C_{Al_2O_3}$ was 2.5%.

The data obtained in this study demonstrate that addition of corundum at low concentrations ($C_{Al_2O_3} \le$ 5%) into the $CaO–ZrO_2$ matrix is accompanied by a negligible increase in the average crystallite size of zirconium dioxide D_{ZrO_2} from 65 to 85 nm (see Table 1). A further rise in corundum concentration (up to 25%) causes no significant changes in D_{ZrO_2}. The average size of corundum grains $D_{Al_2O_3}$ significantly varies from 75 to 120 nm depending on $C_{Al_2O_3}$ (see Table 1). At low corundum concentrations $C_{Al_2O_3} \le 5\%$, we were unable to reliably determine the $D_{Al_2O_3}$ values.

Porosity of $CaO–ZrO_2$ zirconium ceramics (without corundum added) synthesized under the conditions described above is Π = 2.8%. It is important to mention that addition of a minor amount of corundum ($C_{Al_2O_3}$ = 5%) to the zirconium dioxide matrix reduces porosity down to Π = 0.6% (see Table 1). Further increase in corundum concentration (up to 25%) does not significantly alter the composite porosity (Π = 0.3–0.7%).

Hence, the employed synthesis modes yield a $CaO–ZrO_2–Al_2O_3$ ceramic composite with low porosity (Π ~ 0.5%), high content of the tetragonal phase (C_{t-ZrO_2} ~ 95%), and average crystallite size of zirconium dioxide D_{ZrO_2} ~ 85 nm.

Physicomechanical and Tribological Properties

The dependence between microhardness H and corundum concentration $C_{Al_2O_3}$ in the composite is found to be nonlinear (Fig. 2, curve *1*). In the range of corundum concentrations 2.5% ≤ $C_{Al_2O_3}$ ≤ 10%, the dependence $H(C_{Al_2O_3})$ has a singularity. At $C_{Al_2O_3}$ = 5%, microhardness is significantly higher than the H value predicted from the perspective of the additive contribution made by the corundum component of the composite.

The function showing the dependence between fracture toughness K_C of synthesized $CaO–ZrO_2–Al_2O_3$ ceramic composites on corundum concentration $C_{Al_2O_3}$ in them is also not typical (Fig. 2, curve *2*). Maximum fracture toughness K_C of the composites is observed at corundum concentrations 2.5% ≤ $C_{Al_2O_3}$ ≤ 10%. It is important to mention that elevated microhardness and fracture toughness are observed at the same corundum concentrations in the composite (Fig. 2, curves *1* and *2*). The resulting functions $H(C_{Al_2O_3})$ and $K_C(C_{Al_2O_3})$ are consistent with the date reported in [15].

It should be noted that the non-monotonous behavior of the dependence of mechanical properties of a $CaO–ZrO_2–Al_2O_3$ ceramic composite synthesized by low-temperature sintering on corundum concentration is also observed at the macro level. Figure 3 (curve *1*) shows flexural strength σ_C of synthesized $CaO–ZrO_2–Al_2O_3$ composites as a function of corun-

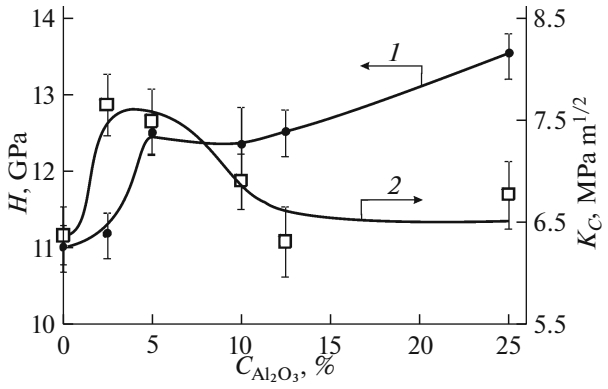

Fig. 2. (*1*) Microhardness and (*2*) fracture toughness of synthesized $CaO–ZrO_2–Al_2O_3$ ceramic composites as functions of corundum concentration $C_{Al_2O_3}$ in them.

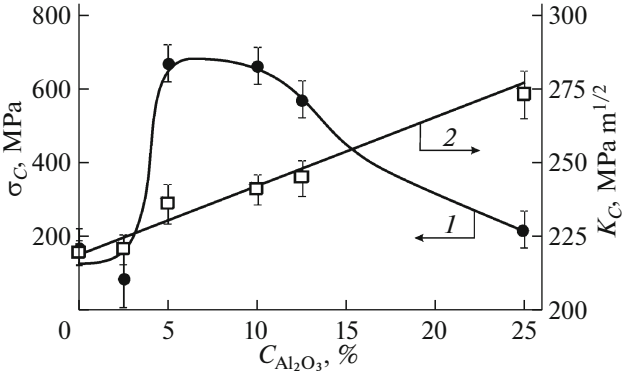

Fig. 3. (*1*) Flexural strength and (*2*) the Young's modulus of the synthesized $CaO–ZrO_2–Al_2O_3$ composites as functions of corundum concentration $C_{Al_2O_3}$ in them.

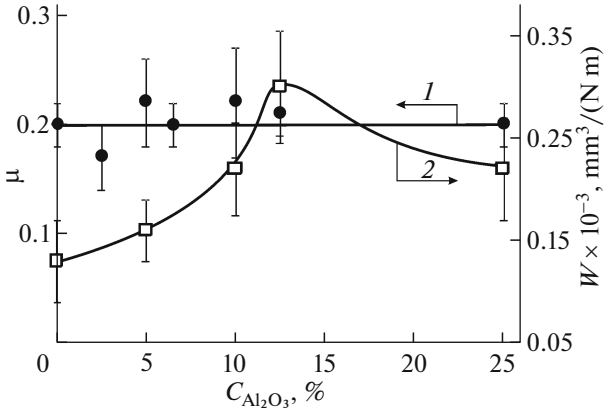

Fig. 4. (*1*) The coefficient of friction and (*2*) wear of synthesized $CaO–ZrO_2–Al_2O_3$ ceramic composites as functions of corundum concentration $C_{Al_2O_3}$ in them.

dum concentration $C_{Al_2O_3}$ in them. The maximum flexural strength ($\sigma_C = 668 \pm 50$ MPa) is reached in the composites containing 5% of corundum.

Hence, a comprehensive analysis of the dependence of microhardness, fracture toughness, and flexural strength on corundum concentration in a $CaO–ZrO_2–Al_2O_3$ composite indicates that the optimal ratio between mechanical properties is reached at corundum concentration $C_{Al_2O_3} = 5\%$. Young's modulus E increases in proportion to the rise in corundum concentration in a $CaO–ZrO_2–Al_2O_3$ composite (Fig. 3, curve *3*). Observed linear dependence $E(C_{Al_2O_3})$ agrees with the literature data [17, 18] and is caused by additive contributions of contents of each component in the composite to the resulting Young's modulus.

Figure 4 (curve *1*) shows the coefficients of friction of the ceramic composites with different corundum contents ($0 \le C_{Al_2O_3} \le 25\%$). One can see that the coefficient of friction is independent of corundum concentration in the composite and remains constant $\mu \approx 0.2$. Meanwhile, the degree of wear as a function of corundum content in a $CaO–ZrO_2–Al_2O_3$ ceramic composite is non-monotonous and has a maximum (Fig. 4, curve *2*). The point to note is that at corundum content in the $CaO–ZrO_2–Al_2O_3$ ceramic composite $C_{Al_2O_3} = 5\%$ (this ratio between $CaO–ZrO_2$ and Al_2O_3 concentrations is optimal in terms of mechanical properties of the composite), the coefficient of friction and wear almost coincide with the corresponding values obtained for $CaO–ZrO_2$ ceramics that contains no corundum. In other words, addition of corundum at concentration $C_{Al_2O_3} = 5\%$ into the $Ca–ZrO_2$ matrix improves the mechanical properties of the material without deteriorating its tribological characteristics.

DISCUSSION

As demonstrated above, the elevation of hardness H of the composite due to redistribution of concentrations of the components is usually accompanied by a decrease in fracture toughness K_C (Fig. 1). In other words, hardness of the $ZrO_2–Al_2O_3$ composites usually goes up as corundum concentration in them is increased, while fracture toughness goes down. The resulting dependences $H(C_{Al_2O_3})$, $K_C(C_{Al_2O_3})$, and $\sigma(C_{Al_2O_3})$ are non-monotonous. The type of dependences listed above is not typical of our combination of the components probably due to sintering conditions. The sintering temperatures used under our experimental conditions ($T_1 = 1300$°C and $T_2 = 1200$°C) are much lower than the ones typically used for thermal treatment of corundum-based ceramics ($T > 1500$°C [6]). On the one hand, this does not allow composite hardness to increase in proportion to the rising Al_2O_3 content in the composite. On the other hand, low-temperature sintering does not significantly increase the average grain size of zirconium dioxide (in our case, $D_{ZrO_2} \le 85$ nm), which has a positive effect on microhardness of the synthesized composites.

Fracture toughness of the $ZrO_2–Al_2O_3$ ceramic composites typically goes down in proportion to corundum content in them. The revealed maxima on $K_C(C_{Al_2O_3})$ and $\sigma_C(C_{Al_2O_3})$ in the range of low corundum concentrations ($C_{Al_2O_3} \sim 5\%$) should probably be attributed to manifestation of the dispersion strengthening mechanism. The SEM data confirm this assumption. Figure 5 shows the SEM images of indents and apices of radial cracks in $CaO–ZrO_2–Al_2O_3$ ceramic composites with corundum contents of 5 and 25% as an example. One can see (Figs. 5b, 5d) that radial cracks propagating along the grain bound-

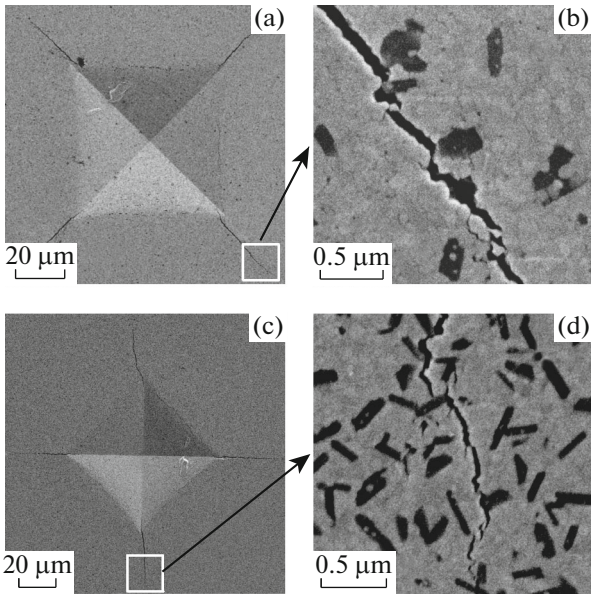

Fig. 5. Typical SEM images of (a, c) the indents and apices of radial cracks (b, d) in $CaO–ZrO_2–Al_2O_3$ ceramic composites with corundum content being (a, b) 5% and (c, d) 25%. The dark areas in the SEM images correspond to inclusions (crystallites) of corundum.

aries occasionally "bump into" Al_2O_3 crystallites that have much larger transverse dimensions (dark areas in the SEM images) as compared to those of ZrO_2 crystallites. This makes cracks deviate from the original propagation direction even at low corundum concentrations ($C_{Al_2O_3} = 5\%$). This phenomenon is accompanied by energy dissipation and a corresponding increase in fracture toughness K_C. The increase in corundum concentration in the composite ($C_{Al_2O_3} = 25\%$) elevates the frequency of deviations of cracks as a result of their "bumping" into Al_2O_3 crystallites (Fig. 5d), which is expected to cause a proportional rise in the K_C value. However, the increase in corundum concentration and the corresponding reduction of content of stabilized zirconium dioxide in the composite decreases the contribution of transformation strengthening intrinsic of $CaO–ZrO_2$. Hence, the reciprocal responses of the effect of corundum concentration on the dispersion and transformation mechanisms of composite strengthening are responsible for the observed non-monotonous behavior (i.e., presence of the maxima) of the dependence between fracture toughness K_C and flexural strength σ_C on corundum concentration $C_{Al_2O_3}$.

CONCLUSIONS

We have studied the structure, phase composition (the ratio between the monoclinic, tetragonal, and cubic ZrO_2 phases), as well as a complex of mechanical and tribological characteristics of $CaO–ZrO_2–Al_2O_3$ ceramic composites synthesized by low-temperature sintering, with corundum content ranging from 0 to 25%. It was found that the best mechanical and tribological properties for these composites (H = 12.48 ± 0.25 GPa, K_C = 7.5 ± 0.35 MPa $m^{1/2}$, σ_C = 668 ± 50 MPa, μ = 0.22 ± 0.04, and $W = 0.16 \times 10^{-3}$ mm^3 N^{-1} m^{-1}) are reached at corundum concentration $C_{Al_2O_3} = 5\%$. The content of the tetragonal phase of zirconium dioxide $C_{t–ZrO_2}$ is equal to 96%; the average crystallite size D_{ZrO_2} is 85 nm; the porosity of the ceramic composite П is 0.6%. Low-temperature sintering and the use of CaO, a relatively inexpensive stabilizer of the tetragonal phase of zirconium dioxide, ensures low cost of the synthesized composites, which is a rather important factor for practical applications.

ACKNOWLEDGMENTS

This study was supported by the Russian Science Foundation (project no. 16-19-10405). The results were obtained using the equipment of the Multiple-Access Center at the Derzhavin Tambov State University.

REFERENCES

1. L.-Sh. Fu, Zh. Wang, X.-S. Fu, G.-Q. Chen, and W.-L. Zhou, Mater. Sci. Eng.: A **703**, 372 (2017). doi 10.1016/j.msea.2017.07.002
2. M. Boniecki, P. Gołbiewski, W. Wesołowski, M. Woluntarski, A. Piatkowska, M. Romaniec, P. Ciepielewski, and K. Krzyà , Ceram. Int. **43**, 10066 (2017). doi 10.1016/j.ceramint.2017.05.025
3. A. Smirnov, J. F. Bartolome, H.-D. Kurland, J. Grabow, and F. A. Muller, J. Am. Ceram. Soc. **99**, 3205 (2016). doi 10.1111/jace.14460
4. V. R. Khrustov, V. V. Ivanov, S. V. Zayats, A. S. Kaygorodov, S. N. Paranin, and S. O. Cholakh, Inorg. Mater.: Appl. Res. **5**, 482 (2014). doi 10.1134/S2075113314050098
5. I. Danilenko, G. Lasko, I. Brykhanova, V. Burkhovetski, and L. Ahkhozov, Nanoscale Res. Lett. **12**, 125 (2017). doi 10.1186/s11671-017-1901-7
6. V. Verma and B. V. Manoj Kumar, Mater. Today: Proc. **4**, 3062 (2017). doi 10.1016/j.matpr.2017.02.189
7. M. Michálek, J. Sedláček, M. Parchoviansky, M. Michálková, and D. Galusek, Ceram. Int. **40**, 1289 (2014). doi 10.1016/j.ceramint.2013.07.008
8. A. Smirnov, J. F. Bartolome, H.-D. Kurland, J. Grabow, and F. A. Muller, J. Am. Ceram. Soc. **99**, 3205 (2016). doi 10.1111/jace.14460
9. M. H. Ghaemi, S. Reichert, A. Krupa, M. Sawczak, A. Zykova, K. Lobach, S. Sayenko, and Y. Svitlychnyi, Ceram. Int. **43**, 9746 (2017). doi 10.1016/j.ceramint.2017.04.150

10. S. E. Porozova and V. B. Kulmetyeva, Inorg. Mater.: Appl. Res. **5**, 420 (2014). doi 10.1134/S2075113314040406

11. S. Sequeira, M. H. Fernandes, N. Neves, and M. M. Almeida, Ceram. Int. **43**, 693 (2017). doi 10.1016/j.ceramint.2016.09.216

12. F. Lange, J. Mater. Sci. **17**, 225 (1982). doi 10.1007/BF00809060

13. F. Zhang, L.-F. Lin, and E.-Z. Wang, Ceram. Int. **41**, 12417 (2015). doi 10.1016/j.ceramint.2015.06.081

14. J. Fan, T. Lin, F. Hu, Y. Yu, M. Ibrahim, R. Zheng, Sh. Huang, and J. Ma, Ceram. Int. **43**, 3647 (2017). doi 10.1016/j.ceramint.2016.11.204

15. A. A. Dmitrievskii, A. I. Tyurin, A. O. Zhigachev, D. G. Guseva, and P. N. Ovchinnikov, Tech. Phys. Lett. **44**, 141 (2018). doi 10.1134/S1063785018020219

16. G. R. Anstis, P. Chantikul, B. R. Lawn, and D. B. Marshall, J. Am. Ceram. Soc. **64**, 533 (1981). doi 10.1111/j.1151-2916.1981.tb10320.x

17. W. Pabst, E. Gregorová, and M. Cerny, J. Eur. Ceram. Soc. **33**, 3085 (2013). doi 10.1016/j.jeurceramsoc.2013.06.012

18. F. Kern and R. Gadow, J. Eur. Ceram. Soc. **32**, 3911 (2012). doi 10.1016/j.jeurceramsoc.2012.03.014

Translated by D. Terpilovskaya